# Diffraction of complex harmonic plane waves and the stimulation of transient leaky Rayleigh waves

Nico F. Declercq[a] and Joris Degrieck
*Soete Laboratory, Department of Mechanical Construction and Production, Ghent University, Sint Pietersnieuwstraat 41, B-9000 Ghent, Belgium*

Oswald Leroy
*Interdisciplinary Research Center, Katholieke Universiteit Leuven Campus Kortrijk, Etienne Sabbelaan 53, B-8500 Kortrijk, Belgium*

(Received 9 March 2005; accepted 24 October 2005; published online 14 December 2005)

This paper describes the interaction of complex harmonic plane waves on a periodically corrugated surface. It is shown that the ability of complex harmonic plane waves to stimulate leaky Rayleigh waves on a corrugated surface is similar to the ability of harmonic inhomogeneous waves to stimulate leaky Rayleigh waves on a smooth interface. Because the experimental generation of harmonic inhomogeneous waves is more complicated and less flexible than the generation of complex harmonic waves, the combination of complex harmonic plane waves with a diffraction grating therefore offers an excellent alternative. The theoretical model developed here is based on the well-known and experimentally verified complex harmonic wave theory and the famous Rayleigh decomposition of the diffracted field. The numerical examples are given for combinations of frequency and corrugation dimensions that justify the use of the Rayleigh theory. A study of the influence of a complex frequency on the generation of Scholte-Stoneley surface waves is performed as well. © *2005 American Institute of Physics*. [DOI: 10.1063/1.2137885]

## INTRODUCTION

In the 1980s, a lot of attention was paid to the use of Scholte-Stoneley waves for nondestructive testing purposes. Such waves possess the important feature of propagation along a solid-liquid interface with only minor damping, because their velocity is lower than the velocity of sound in the bulk of both surrounding media. Therefore no radiation occurs. In other words, Scholte-Stoneley waves are excellent tools for long-distance nondestructive testing. The main problem, however, is their experimental generation. The same reason they do not radiate into the surrounding media is the reason they cannot be generated by means of incident sound, at least not on smooth surfaces. One method to resolve this problem is the use of a periodically corrugated surface. Then, Scholte-Stoneley waves can be generated by means of diffraction. This phenomenon has been studied in great extent before.[1–9] In this paper, we use the term harmonic (homogeneous) plane wave for a classical sinusoidal plane wave, i.e., a plane wave determined by a real wave vector and a real frequency. When the wave vector is complex valued, we use the term "inhomogeneous wave" or "harmonic inhomogeneous wave." Furthermore, we use the term "complex harmonic plane wave" for the case when the frequency is complex valued and the wave vector is real. For complex harmonic plane waves having a complex valued wave vector as well, we explicitly use the term "complex harmonic inhomogeneous wave." It is widely accepted that it is possible to stimulate leaky Rayleigh waves on smooth interfaces by means of harmonic inhomogeneous waves incident at the Rayleigh angle.[10–14] Harmonic inhomogeneous waves are plane waves whose amplitude shows exponential decay along the wave front, but not in the time domain. Furthermore, similar to the case of smooth interfaces, these waves are able to stimulate leaky Rayleigh waves on periodically corrugated surface for normal incidence.[15–19] The main problem, however, has always been that the experimental generation of inhomogeneous waves is not quite convenient. More precisely, all methods of generation are based on rigid and complicated experimental setups and are expensive and time consuming,[16,19,20] because for each requested inhomogeneous wave, a different experimental configuration is necessary.

The generation of a complex harmonic plane wave is simpler and is much more flexible.[21–26] The theoretical model and the numerical simulations in this paper are based on two well-established theories, i.e., the theory of complex harmonic waves and the Rayleigh theory of sound diffraction on periodically rough surfaces. The theory of complex harmonic waves is based on complex solutions of the wave equation; they have also been generated experimentally.[21–26] The Rayleigh theory of sound diffraction on periodically rough surfaces, is also well established and is actually a simplified approach of more complicated models such as the differential[27,28] and integral equation approach[29–33] and the Waterman theory.[34–38] We apply the Rayleigh theory because of two important reasons: First the theory is convenient to take into account complex harmonic and inhomogeneous waves; second, it has been shown by Wirgin[39] that "contrary to prevailing opinion, the Rayleigh theory is fully capable of describing the scattering phenomena produced by a wide

[a]Author to whom correspondence should be addressed; Postdoctoral fellow of the research foundation—Flanders (FWO-Vlaanderen); electronic mails: nicof.decleracq@ugent.be and declercq@ieee.org

 

TABLE I. Different plane-wave definitions depending on the values of **k** and $\omega$.

| **k** | $\omega$ | Nomenclature |
|---|---|---|
| Real | Real | Harmonic (homogeneous) plane wave |
| Real | Complex | Complex harmonic (homogeneous) plane wave |
| Complex | Real | (Harmonic) inhomogeneous wave |
| Complex | Complex | Complex harmonic inhomogeneous wave |

class of corrugated surfaces, including those whose roughness is rather large." Furthermore, Wirgin[39] proves that the Rayleigh theory is valid, for $\lambda$ the largest wavelength involved in the diffraction phenomenon, for $\Lambda$ the corrugation period, and for $h$ the corrugation height, whenever

$$h < 0.34\Lambda, \tag{1}$$

and

$$\lambda > 1.533\,48h. \tag{2}$$

The diffraction model as is used here has been applied recently for the explanation of the backward beam displacement[40,41] and has been extended recently in order to simulate diffraction effects for audible sound at the great pyramid of Chichen Itza in Mexico.[42] An extension to two-dimensional corrugations has also been proposed before.[43]

In this paper it will be shown that similar to harmonic inhomogeneous waves,[44] complex harmonic waves are excellent tools for stimulating (transient) leaky Rayleigh waves on periodically corrugated surfaces. Furthermore, it will be shown that this stimulation effect is absent on smooth surfaces.

## I. TRANSIENT HARMONIC PLANE WAVES

It is well known that plane waves are a solution of the wave equation in viscoelastic media.[25] Plane waves are described by a displacement vector **u** as follows:

$$\mathbf{u} = A\mathbf{P}\exp(i\mathbf{k}\cdot\mathbf{r} - i\omega t). \tag{3}$$

Besides time $t$ and space **r**, all parameters in (3), i.e., the amplitude $A$, the polarization **P**, the wave vector **k**, and the angular frequency $\omega$ can be complex valued.[21–25] The nomenclature for the different kinds of possible plane waves is found in Table I. In the case that

$$\omega = \omega_1 + i\omega_2, \tag{4}$$

and

$$\mathbf{k} = \mathbf{k}_1 + i\mathbf{k}_2 = \mathbf{k}_1 + i(\alpha - \beta), \tag{5}$$

with $\alpha \| \mathbf{k}_1$ and $\beta \perp \mathbf{k}_1$, it can be verified that

$$\mathbf{u} = A\mathbf{P}\exp(\omega_2 t)\exp(-\alpha\cdot\mathbf{r})\exp(\beta\cdot\mathbf{r})\exp i(\mathbf{k}_1\cdot\mathbf{r} - \omega_1 t). \tag{6}$$

In (6) it is noticed that $\mathbf{k}_1$ and $\omega_1$ influence the vibration itself, while all other parameters influence the amplitude attributed to that vibration. The parameter $\mathbf{k}_1$ is called the propagation wave vector, $\omega_1$ is the real angular frequency, $\alpha$ is called the damping vector, while $\beta$ is called the inhomogeneity vector. The parameter $\omega_2$ determines the transient

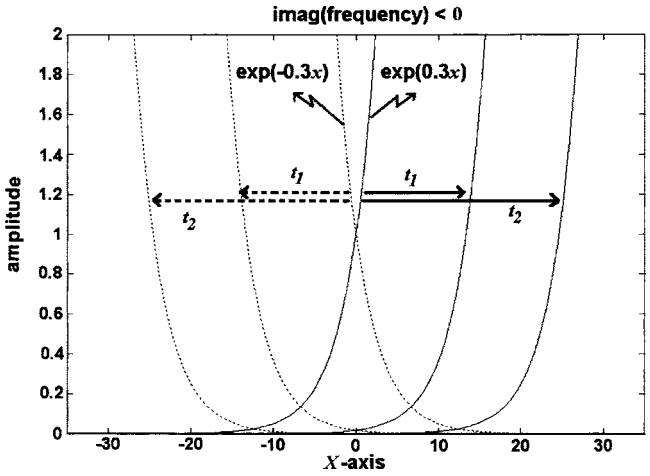


FIG. 1. Schematic view of the amplitude migration that occurs, as time passes, of a complex harmonic inhomogeneous wave. The amplitude along the wave front is depicted at different instants and for positive and negative inhomogeneities.

feature of the wave under consideration and is called the source parameter. If it is positive, the wave is amplified in time, and if it is negative, the wave diminishes in time. Important to note is that (6) shows that the amplitude of **u** changes instantaneously throughout space. If for each instant of time the amplitude would be the same everywhere, then an instantaneous change throughout space would be a violation of the principle of energy conservation (energy cannot just vanish or appear) and also a violation of the fact that no signal can ever be transported faster than the speed of light under the assumption that time and space are real quantities. Therefore, it is necessary to demand that expression (3) must be a solution of the wave equation.[21–25] For viscoelastic media, this means that the dispersion relation must hold,[21–25] i.e.,

$$\mathbf{k}\cdot\mathbf{k} = \left(\frac{\omega}{\nu_b} + i\alpha_{0,b}\right)^2, \tag{7}$$

where $b=d$ for longitudinal waves or $b=s$ for shear waves. $\nu_b$ is the phase velocity for harmonic homogeneous plane waves (i.e., having a real wave vector and a real frequency) and $\alpha_{0,b}$ is the intrinsic damping coefficient.

It is precisely this dispersion relation that relates the phase velocity and the amplitude distribution in space to the real angular frequency $\omega_1$ and the source parameter $\omega_2$. Even though the effect of (7) on sound waves is mathematically covered in Refs. 21–25, it is interesting to find out what the physical consequences are. The effect of (7) on a transient wave with respect to time is the description of the amplitude migration in space as a function of time. Consider a transient plane wave having an inhomogeneity vector $\beta$ different from zero and propagating along the $z$ axis. Then, if we plot the amplitude along the $x$ axis as a function of time, we get something like in Fig. 1 where the amplitude changes exponentially along the $x$ axis due to $\beta$, but also changes exponentially in time. This amplitude change in time can easily be interpreted as a position shift in time to the right or to the left, depending on the value of $\omega_2$ and the inhomogeneity $\beta$. Therefore the effect of $\omega_2$ should be interpreted as the effect

of lateral amplitude migration in time. In the case that also $\alpha$ differs from zero, this amplitude migration also occurs in the direction of phase propagation.

If $\beta=0$ then the dispersion relation makes sure that $\alpha$ differs from zero, where there is amplitude migration along the phase propagation direction. This amplitude migration prevents physical impossibilities such as magical (dis)appearance of energy as described before.

Whenever sound is transmitted/reflected at a smooth interface between two different media, it is necessary to determine in what direction the vector $\mathbf{k}$ is pointing for each of the generated waves. For smooth surfaces, the lateral direction is always determined by the well-known generalized Snell's law, which states that along the interface there is continuity of the complex wave vector and that the complex frequency remains unchanged,[25] but the component perpendicular to the interface must be chosen carefully. We will show that this choice must be performed with consideration of the energy propagation no matter what this means for the wave vector itself. The reason is that the wave vector itself is not of primordial importance to determine what happens to a sound wave, because amplitude migration due to the source parameter $\omega_2$ must be considered as well. For that reason it is convenient to work with the following slowness vector:

$$\mathbf{k} = \omega \mathbf{S}, \tag{8}$$

where

$$\begin{aligned} \mathbf{k}_1 &= \omega_1 \mathbf{S}_1 - \omega_2 \mathbf{S}_2, \\ \mathbf{k}_2 &= \omega_2 \mathbf{S}_1 + \omega_1 \mathbf{S}_2. \end{aligned} \tag{9}$$

It has been shown by Deschamps *et al.*[22] that the vector corresponding to the energy velocity is given by

$$\mathbf{v}_E = \frac{\mathbf{S}_1}{\mathbf{S}_1 \cdot \mathbf{S}_{\mathrm{ph}}}, \tag{10}$$

with the phase slowness vector $\mathrm{S}_{\mathrm{ph}}$ given by

$$\mathbf{S}_{\mathrm{ph}} = \frac{\mathbf{k}_1}{\omega_1}. \tag{11}$$

This shows that the energy propagates in the direction of $\mathbf{S}_1$, i.e.,

$$\mathbf{v}_E \simeq \frac{\mathbf{k}_2 \omega_2 + \omega_1 \mathbf{k}_1}{\omega_1^2 + \omega_2^2}. \tag{12}$$

From a numerical point of view, if one considers dispersion relation (7) and also Snell's law for smooth interfaces (or the grating equation in the case of corrugated surfaces, see further below), only the exact value of the wave vector of diffracted waves along the interface is determined. For the component perpendicular to the interface only the complex magnitude is determined and not the sign that is to be attributed to that magnitude. For inhomogeneous waves having a real frequency, this choice has been discussed and determined before,[17,45–48] i.e., reflected waves must always propagate away from the interface, while the same holds for transmitted waves, given the fact that the reflected companion (of the same order $m$) propagates at an angle below the critical angle for the transmitted wave under consideration. If this reflected companion propagates at an angle beyond the critical angle, then the transmitted wave under consideration must propagate towards the interface. Furthermore, whenever a diffracted wave is evanescent, i.e., having a real wave-vector component along the interface and an imaginary wave-vector component perpendicular to the interface, then exponential amplitude decay away from the interface must be imposed.[1,6] For the case of transient waves, we have translated all of these sign choice principles to energy propagation directions instead of just (phase) propagation directions. We have then adapted the sign choice of the wave vector to the correct corresponding sign choice of the energy propagation vector. The reason is that the real part of the wave vector does not determine the energy propagation on its own (as in the case of harmonic inhomogeneous plane waves in isotropic media), but only in combined action with the source term $\omega_2$.

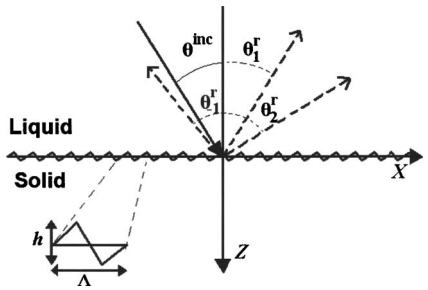


FIG. 2. Schematic view of the considered corrugated interface. The different reflection angles are schematically shown for different diffraction orders and for obliquely incident sound.

## II. THE SYSTEM OF EQUATIONS

### A. Description of the incident and the diffracted wave fields

Consider a periodically corrugated interface between a liquid and a solid as depicted in Fig. 2. The corrugation is periodic with period $\Lambda$ and is given by

$$g(x,z) = f(x) - z = 0 = g(x+\Lambda, z). \tag{13}$$

We take into account the Rayleigh decomposition[1–9,15–19,39,49,50] of the diffracted wave field and also the characteristics of longitudinal and shear waves, where the displacement of the incident waves $\mathbf{N}^{\mathrm{inc}}$, the (longitudinal) reflected waves $\mathbf{N}^r$, and the longitudinal and shear waves in the solid $\mathbf{N}^d$ and $\mathbf{N}^s$, respectively, are written as

$$\mathbf{N}^{\mathrm{inc}} = A^{\mathrm{inc}} \varphi^{\mathrm{inc}} \left( i k_x^{\mathrm{inc}} \mathbf{e}_x + i k_z^{\mathrm{inc}} \mathbf{e}_z \right), \tag{14}$$

$$\mathbf{N}^r = \sum_m A_m^r \varphi^{m,r} \left( i k_x^{m,r} \mathbf{e}_x + i k_z^{m,r} \mathbf{e}_z \right), \tag{15}$$

$$\mathbf{N}^d = \sum_m A_m^d \varphi^{m,d} \left( i k_x^{m,d} \mathbf{e}_x + i k_z^{m,d} \mathbf{e}_z \right), \tag{16}$$

$$\mathbf{N}^s = \sum_m A_m^s \mathbf{P}^{m,s} \varphi^{m,s}, \tag{17}$$

with

$$\varphi^{\zeta} = \exp i\left(\mathbf{k}^{\zeta} \cdot \mathbf{r}\right), \tag{18}$$

and

$$k_x^{m,s} P_x^{m,s} + k_y^{m,s} P_y^{m,s} + k_z^{m,s} P_z^{m,s} = 0. \tag{19}$$

The index "$m$" denotes the diffraction order and $\zeta$ represents "inc," "$m,r$," "$m,d$," or "$m,s$." The properties of transient waves as described in the previous paragraph are taken into account, except for Snell's law. When diffraction occurs, Snell's law must be replaced by the generalized grating equation:[15–19,25]

$$k_x^{m,b} = k_x^{\mathrm{inc}} + m\frac{2\pi}{\Lambda}, \tag{20}$$

with $b=r$ for the reflected field in the liquid and $b=d$ or $b=s$ for the transmitted longitudinal and shear waves in the solid, respectively. Equation (20) shows that only the real part of the lateral wave-vector component is affected by the grating, not the imaginary part, whereas if we rewrite (20) in the slowness vector components [see (8)),

$$S_{1,x}^{m,b} = S_{1,x}^{\mathrm{inc}} + m\frac{2\pi\omega_1}{\Lambda\left(\omega_1^2 + \omega_2^2\right)}, \tag{21}$$

$$S_{2,x}^{m,b} = S_{2,x}^{\mathrm{inc}} - m\frac{2\pi\omega_2}{\Lambda\left(\omega_1^2 + \omega_2^2\right)}. \tag{22}$$

Equation (22) shows that the imaginary part of the lateral component of the slowness vector is affected by the grating.

To summarize, each wave in the Rayleigh decomposition of the diffracted field is characterized by a wave-vector component along the interface determined by grating equation (20) and a wave-vector component perpendicular to the interface, having a value determined by the wave equation [through dispersion relation (7)] and a sign determined by the causality principle. However, each wave must also have an amplitude that is determined by continuity conditions. This is explained in the next section.

### B. The continuity conditions

In the media $\tau$ ($\tau=1$ in the liquid and $\tau=2$ in the solid) the stress tensor $T^{\tau}$ is given[51,52] by its elements,

$$T_{ij}^{\zeta} = \sum_{\eta}\left(\lambda_1^{\tau} + \lambda_2^{\tau}\frac{\partial}{\partial t}\right)\varepsilon_{\eta\eta}^{\tau}\delta_{i,j} + 2\left(\mu_1^{\tau} + \mu_2^{\tau}\frac{\partial}{\partial t}\right)\varepsilon_{i,j}^{\tau}, \tag{23}$$

in which the strain tensor $\varepsilon_{ij}^{\tau}$ is

$$\varepsilon_{ij}^{\tau} = \frac{1}{2}\left(\partial_i N_j^{\tau} + \partial_j N_i^{\tau}\right). \tag{24}$$

The Lamé constants are denoted by $\lambda_1^{\tau}$ and $\mu_1^{\tau}$, while the viscosity coefficients are given by $\lambda_2^{\tau}$ and $\mu_2^{\tau}$. They accomplish dispersion relation (7) if

$$\mathbf{k}^{\zeta}\cdot\mathbf{k}^{\zeta} = \frac{\rho\omega^2}{\left(\lambda_1^{\tau} - i\omega\lambda_2^{\tau}\right) + 2\left(\mu_1^{\tau} - i\omega\mu_2^{\tau}\right)} = \left(\frac{\omega}{\nu_d} + i\alpha_{0,d}\right)^2, \tag{25}$$

for longitudinal waves ($\zeta$=inc or $m,r$ in the liquid and $\zeta=m,d$ or $m,s$ in the solid) and if

$$\mathbf{k}^{\zeta}\cdot\mathbf{k}^{\zeta} = \frac{\rho\omega^2}{\left(\mu_1^{\tau} - i\omega\mu_2^{\tau}\right)} = \left(\frac{\omega}{\nu_s} + i\alpha_{0,s}\right)^2, \tag{26}$$

for shear waves ($\zeta=s$, 2 in the solid). In order to find the unknown coefficients $A_m^r$, $A_m^d$, $A_m^s P_x^{m,s}$, $A_m^s P_y^{m,s}$, and $A_m^s P_z^{m,s}$, the equations that describe the continuity of normal stress and strain along interface (13) need to be solved, i.e.,

$$\left(\mathbf{N}^{\mathrm{inc}} + \mathbf{N}^{r}\right)\cdot\nabla g = \left(\mathbf{N}^{d} + \mathbf{N}^{s}\right)\cdot\nabla g, \quad \text{along } g = 0, \tag{27}$$

$$\sum_j T_{ij}^1 (\nabla g)_j = \sum_j T_{ij}^2 (\nabla g)_j \quad \text{along } g = 0, \tag{28}$$

and also because for shear waves the complex displacement is perpendicular to the complex wave vector,

$$\left(A_m^s P_x^{m,s} k_x^{m,s} + A_m^s P_y^{m,s} k_y^{m,s} + A_m^s P_z^{m,s} k_z^{m,s}\right)\varphi^{m,s} = 0. \tag{29}$$

Conditions (27)–(29) lead to five equations that are periodic in $x$, where a sufficient condition for a correct solution is that the Fourier coefficients (for a discrete Fourier transform over the interval $[0\rightarrow\Lambda]$) of the left and right sides of the equations are equal to each other. The wave vectors that are introduced by this discrete Fourier transform are denoted by the order "$p$."

The five equations for each integer $p$ are as follows.

(i) Equation 1

$$\begin{aligned} &A^{\mathrm{inc}} I^{\mathrm{inc},p} i\left(-\mathbf{k}^{\mathrm{inc}}\cdot\mathbf{k}^{\mathrm{inc}} + k_x^{\mathrm{inc}} k_{x,p}\right) \\ &\quad + \sum_m A_m^r I^{m,r,p} i\left(-\mathbf{k}^{\mathrm{inc}}\cdot\mathbf{k}^{\mathrm{inc}} + k_x^m k_x^p\right) \\ &\quad + \sum_m A_m^d I^{m,d,p} i\left(\mathbf{k}^{d,2}\cdot\mathbf{k}^{d,2} - k_x^m k_x^p\right) \\ &\quad - \sum_m A_m^s P_x^{m,s} I^{m,s,p}\left(k_x^p - k_x^m\right) \\ &\quad + \sum_m A_m^s P_z^{m,s} I^{m,s,p}\left(k_z^{m,s}\right) = 0. \end{aligned} \tag{30}$$

(ii) Equation 2

$$
\begin{aligned}
&-A^{\mathrm{inc}} I^{\mathrm{inc},p} \rho_1 \left(k_x^p - k_x^{\mathrm{inc}}\right) - \sum_m A_m^r I^{m,r,p} \rho_1 \left(k_x^p - k_x^m\right) \\
&\quad + \sum_m A_m^d I^{m,d,p} \rho_2 \left( - k_x^m + \left[ 1 + 2 \frac{\left(k_x^m\right)^2 - \mathbf{k}^{d,2} \cdot \mathbf{k}^{d,2}}{\mathbf{k}^{s,2} \cdot \mathbf{k}^{s,2}} \right] k_x^p \right) \\
&\quad + \sum_m A_m^s P_x^{m,s} I^{m,s,p} i \rho_2 \left[ 1 - \frac{k_x^m k_x^p}{\mathbf{k}^{d,2} \cdot \mathbf{k}^{d,2}} + \left( \frac{1}{\mathbf{k}^{d,2} \cdot \mathbf{k}^{d,2}} - \frac{1}{\mathbf{k}^{s,2} \cdot \mathbf{k}^{s,2}} \right) \left(k_x^m\right)^2 \right] \\
&\quad + \sum_m A_m^s P_z^{m,s} I^{m,s,p} \rho_2 i \left(k_z^{m,s}\right) \left[ \left( \frac{1}{\mathbf{k}^{d,2} \cdot \mathbf{k}^{d,2}} - \frac{1}{\mathbf{k}^{s,2} \cdot \mathbf{k}^{s,2}} \right) k_x^m - \left( \frac{1}{\mathbf{k}^{d,2} \cdot \mathbf{k}^{d,2}} - \frac{2}{\mathbf{k}^{s,2} \cdot \mathbf{k}^{s,2}} \right) k_x^p \right] = 0.
\end{aligned} \tag{31}
$$

(iii) Equation 3

$$
+ \sum_m A_m^s P_y^{m,s} I^{m,s,p} i \rho_2 \left( 1 - \frac{k_x^m k_x^p}{\mathbf{k}^{s,2} \cdot \mathbf{k}^{s,2}} \right) = 0. \tag{32}
$$

(iv) Equation 4

$$
\begin{aligned}
&+ A^{\mathrm{inc}} I^{\mathrm{inc},p} \rho_1 k_z^{\mathrm{inc}} e^{-i k_z^{\mathrm{inc}} z_0} + \sum_m A_m^r I^{m,r,p} \left(k_z^{m,r}\right) \rho_1 \\
&\quad + \sum_m A_m^d I^{m,d,p} \left(k_z^{m,d}\right) \rho_2 \left[ - 1 + \frac{2}{\mathbf{k}^{s,2} \cdot \mathbf{k}^{s,2}} \left(k_x^m k_x^p\right) \right] \\
&\quad + \sum_m A_m^s P_x^{m,s} I^{m,s,p} i \left(k_z^{m,s}\right) \rho_2 \left[ \left( \frac{1}{\mathbf{k}^{d,2} \cdot \mathbf{k}^{d,2}} - \frac{1}{\mathbf{k}^{s,2} \cdot \mathbf{k}^{s,2}} \right) k_x^m - \frac{k_x^p}{\mathbf{k}^{s,2} \cdot \mathbf{k}^{s,2}} \right] \\
&\quad + \sum_m A_m^s P_z^{m,s} I^{m,s,p} i \rho_2 \left[ \left( \frac{1}{\mathbf{k}^{d,2} \cdot \mathbf{k}^{d,2}} - \frac{1}{\mathbf{k}^{s,2} \cdot \mathbf{k}^{s,2}} \right) \left(k_z^{m,s}\right)^2 + 1 - \frac{k_x^m k_x^p}{\mathbf{k}^{s,2} \cdot \mathbf{k}^{s,2}} \right] = 0.
\end{aligned} \tag{33}
$$

(v) Equation 5

$$
\left( A_m^s P_x^{m,s} k_x^{m,s} + A_m^s P_y^{m,s} k_y^{m,s} + A_m^s P_z^{m,s} k_z^{m,s} \right) \delta_{m,p} = 0, \tag{34}
$$

with

$$
I^{\mathrm{inc},\eta} = \frac{1}{k_z^{\mathrm{inc}}} \int_\Lambda \exp i \left\{ \left( k_x^{\mathrm{inc}} - k_x^\eta \right) x + \left[ k_z^{\mathrm{inc}} f(x) \right] \right\} dx, \tag{35}
$$

$$
I^{m,\xi,\eta} = \frac{1}{k_z^{m,\xi}} \int_\Lambda \exp i \left[ \left( k_x^m - k_x^\eta \right) x + k_z^{m,\xi} f(x) \right] dx. \tag{36}
$$

For $\delta_{m,p}$ is the Kronecker's delta. It is already seen from (32) that

$$
A_m^s P_y^{m,s} = 0. \tag{37}
$$

Hence $u_y = 0$ and therefore there are no horizontally polarized waves generated. Note that $f(x)$ only appears in the exponentials of the integrals (35) and (36). This is due to the use of partial integration for integrals containing $df/dx$ during equalization of the Fourier coefficients.[1]

### C. Truncation of infinite summations

The linear set of Eqs. (30)–(34) is infinite because $m, p$ may take every possible integer value from $-\infty \rightarrow +\infty$. However, it has been shown before[2,8,9] that the interval of integers may be truncated to $(-N, -N+1, \ldots, N-1, N)$, for $N$ larger than 6.

From Refs. 49 and 53, it is known that for a sawtooth profile,

$$
f(x) = \frac{2hx}{\Lambda} - \frac{h}{2}, \quad \text{if } 0 \leqslant x < \frac{\Lambda}{2}, \tag{38}
$$

$$
f(x) = \frac{3h}{2} - \frac{2hx}{\Lambda}, \quad \text{if } \frac{\Lambda}{2} \leqslant x < \Lambda, \tag{39}
$$

the integrals (35) and (36) become

$$
I^{\mathrm{inc},\eta} = ih\Lambda e^{-ihk_z^{\mathrm{inc}}/2} \frac{1 - (-1)^{-\eta} e^{ihk_z^{\mathrm{inc}}}}{\left(hk_z^{\mathrm{inc}}\right)^2 - (\pi\eta)^2}, \tag{40}
$$

$$
I^{m,\eta,\xi} = ih\Lambda e^{-ihk_z^{\mathrm{inc}}/2} \frac{1 - (-1)^{(m-\eta)} e^{ihk_z^{m,\xi}}}{\left(hk_z^{m,\xi}\right)^2 - \pi^2 (m-\eta)^2}. \tag{41}
$$

In this work, only sawtooth profiles (38) and (39) have been taken under consideration, but the model equally works for other shapes as well.

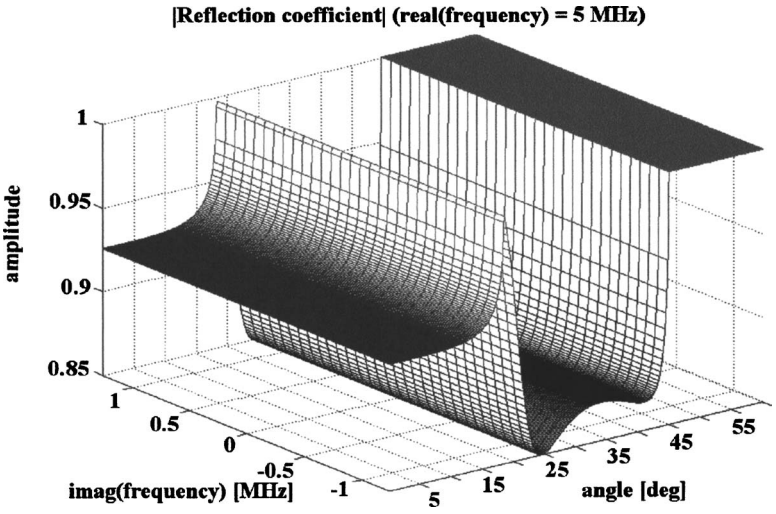


FIG. 3. The absolute value of the reflection coefficient on a smooth water-brass interface, constant real frequency, and different imaginary frequencies. The Rayleigh angle is 48°.

## III. THE NEED FOR DIFFRACTION

In many (NDT) applications, it is desirable to generate surface waves. It is well known that for most liquid-solid interfaces Scholte-Stoneley waves cannot be generated by means of incident sound because their velocity is too low compared with the sound velocities in the surrounding media. One of the techniques that can be used to stimulate Scholte-Stoneley waves is the use of a periodic corrugation on the surface. Then, Scholte-Stoneley waves can be generated under the right conditions by means of diffraction. Even though this has been very successful for relatively wide beams, this success was not shared for the stimulation of leaky Rayleigh waves. It has been shown by Briers and co-workers[15–19,25] that inhomogeneous waves are needed in order to really stimulate leaky Rayleigh waves. Furthermore it is also known that the amplitude of this stimulation will never exceed the one occurring by means of obliquely incident inhomogeneous waves on a plane interface at the Rayleigh angle. Hence the question may arise: Why would anyone apply a diffraction grating to stimulate leaky Rayleigh waves if this can be better accomplished on a plane surface? The answer is simple: A diffraction grating in combination with complex harmonic homogeneous waves has a similar effect as the use of harmonic inhomogeneous waves incident on a smooth interface. As an introduction to this matter, we have calculated the reflection coefficient (on a smooth interface) as a function of the angle of incidence for a constant real frequency and a variable imaginary frequency. This has been done for incident complex harmonic plane waves. Before it has been shown that such waves show exponential amplitude variation along the wave propagation direction. Therefore the imaginary wave vector is directed parallel with the propagation wave vector which is not the structure that a typical leaky Rayleigh wave consists of.[10–14] Furthermore this structure is maintained after reflection due to the dispersion relation and Snell's law. It is therefore unlikely that any actual leaky Rayleigh wave stimulation might occur, as would have been the case if harmonic inhomogeneous waves had been considered.[10–14] The result is shown in Fig. 3 for a water-brass interface and for a real frequency of 5 MHz and different imaginary frequencies. The material properties for water and brass are listed in Table II. For simplicity we have neglected intrinsic damping in the numerical examples. It is verified that the amplitude of the reflection coefficient is independent of the imaginary frequency and it is certainly learned from Fig. 3 that no typical amplitude peaks arise as in the case of harmonic inhomogeneous waves.[10–14]

In Fig. 4 the two Cartesian components of the particle displacement are shown relative to the incident particle displacement amplitude, for a Rayleigh angle of incidence (48°) at 5 MHz and without any transient feature. It is seen that the $z$ component reaches a value of approximately 1.5. This height is independent of the imaginary frequency that is used. We keep this pattern in mind as a reference for further discussions. This amplitude is so low because there is no leaky feature in the liquid side—a feature that is necessary for generating leaky Rayleigh waves.

TABLE II. Material properties used in this work.

| Material | $\rho$ (kg/m$^3$) | $\nu_d$ (m/s) | $\nu_s$ (m/s) |
|---|---|---|---|
| Water | 1000 | 1480 | 0 |
| Brass | 8100 | 4700 | 2100 |

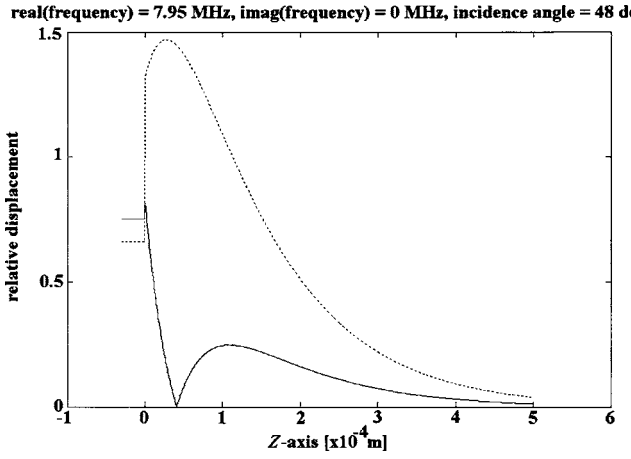


FIG. 4. Relative displacement amplitude for transmitted and reflected sound resulting from harmonic homogeneous plane waves incident on a smooth water-brass interface at the Rayleigh angle. Solid line: $|\mathbf{u}_x|$; dotted line: $|\mathbf{u}_z|$. A typical Rayleigh wave profile is noticeable in the solid.

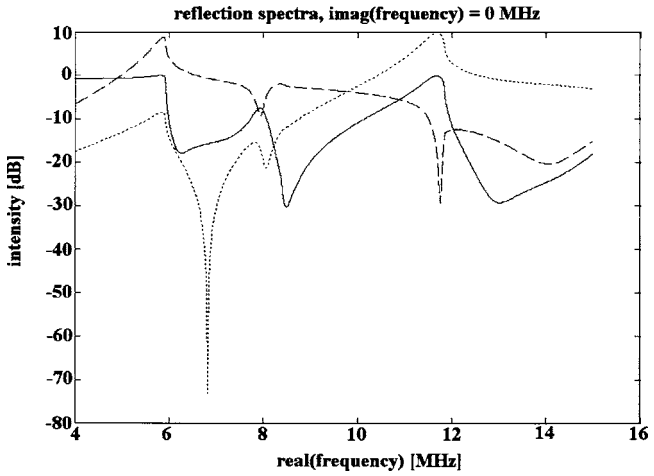


FIG. 5. Diffraction spectra (in dB) of different orders for normal incident harmonic homogeneous plane waves. Solid line: $|A_0^r|^2$; dashed line: $|A_{\pm 1}^r|^2$; dotted line: $|A_{\pm 2}^r|^2$.

Now we study results obtained for diffraction on a periodically rough surface. All diffraction spectra tackled in this paper are performed for normal incidence on a water/brass periodically corrugated interface having a periodicity $\Lambda = 250\ \mu$m and a height $h = 66\ \mu$m. According to (1) and (2) and the material properties given in Table II, this means that the applied Rayleigh theory for diffraction is valid within the frequency interval [4 MHz, 15 MHz]. Furthermore, dispersion equations (25) and (26) must be taken into account and so must grating equation (20), in order to ensure the physical validity of the approach. In Fig. 5 the calculated reflection spectra are shown for normal incident harmonic plane waves. It is seen, for example, that the zero-order reflection coefficient is a function of the incident frequency. This figure corresponds to Fig. 4 in the work of Claeys *et al.*[1] In Figs. 6–8 these spectra are shown not only as a function of the real frequency, but also as a function of the imaginary frequency. In Figs. 9 and 10 the propagation direction is shown for first-order reflected waves. Figure 9 shows the phase propagation direction whereas Fig. 10 shows the energy propagation direction. Noteworthy is the fact that the imaginary frequency has a steering effect on reflected waves. For example, below 6 MHz first-order reflected waves are completely evanescent, which means that their wave-vector component perpendicular to the surface is completely imaginary. This also means that these waves "propagate" along the interface. Figure 9 shows that this evanescence is broken through if complex frequencies are used. For high imaginary frequencies, first-order reflected waves below 6 MHz can perfectly be "erected" and propagate in the bulk instead of being evanescent. Nevertheless, this statement is only true if the phase propagation direction is considered. The energy still flows parallel with the interface, as can be seen in Fig. 10.

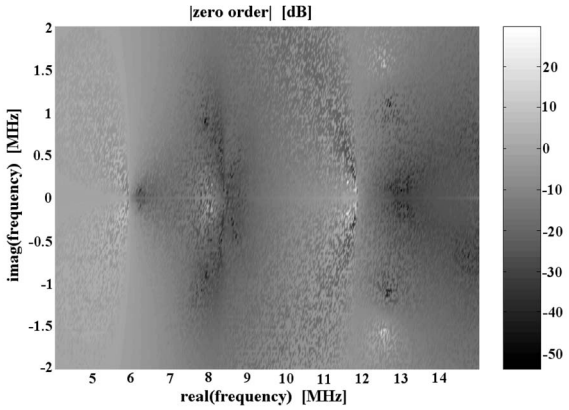


FIG. 6. Diffraction spectra of the zero-order reflected sound ($|A_0^r|^2$ in dB) as a function of the real and imaginary frequencies.

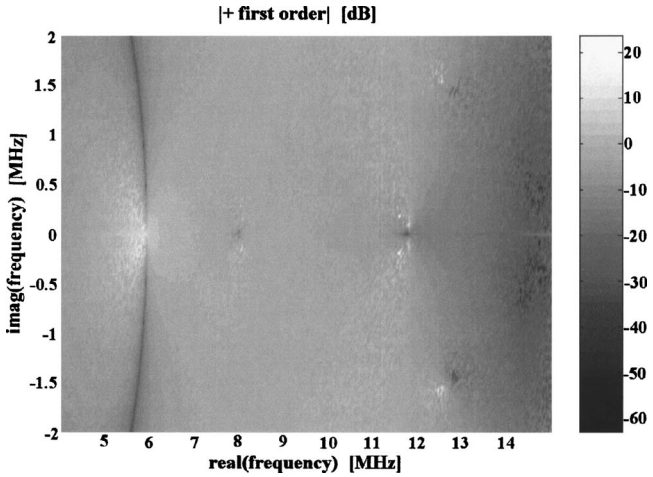


FIG. 7. Diffraction spectra of the first-order reflected sound ($|A_{\pm 1}^r|^2$ in dB) as a function of the real and imaginary frequencies.

## IV. THE STIMULATION OF TRANSIENT SCHOLTE-STONELEY WAVES

In Fig. 5 it is seen that the zero-order reflected sound shows some strong amplitude dips. When these dips are associated with the generation of Scholte-Stoneley waves, they are called the Wood anomalies. It is known from earlier works[1,4] that the anomaly near 5.83 MHz corresponds to first-order diffracted Scholte-Stoneley waves, while the one at double that value corresponds to generated second-order Scholte-Stoneley waves. Figure 11 shows the particle displacement components relative to the displacement ampli-

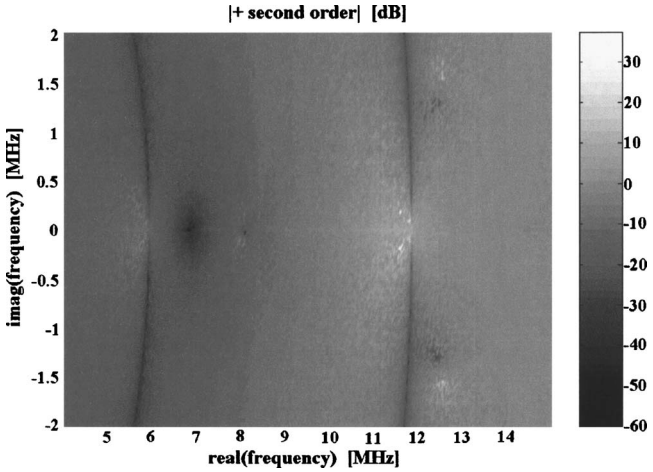


FIG. 8. Diffraction spectra of the second-order reflected sound ($|A_{\pm 2}^r|^2$ in dB) as a function of the real and imaginary frequencies.

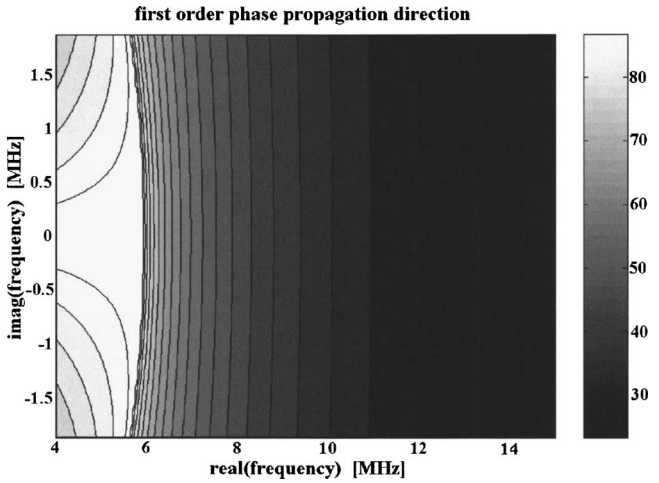


FIG. 9. Phase propagation direction of the first-order reflected waves.

tude of incident waves at 5.83 MHz and with no imaginary frequency component. This is a typical Scholte-Stoneley wave pattern. Most of the amplitude of a Scholte-Stoneley wave is situated in the liquid. In Fig. 6, it can be seen that in the vicinity of 5.83 MHz there are regions with a lower amplitude than the first Wood anomaly. We have studied these stronger anomalies. Figure 12 shows again the displacement pattern for one of those anomalies, i.e., the one at a real frequency of 6.18 MHz and an imaginary frequency of 0.03 MHz. It is seen that something comparable is visible as in Fig. 11. However, the amplitude is much smaller and the wave extends much further into the liquid than its harmonic counterpart. Probably this wave should be called a transient Scholte-Stoneley wave, which is different from a harmonic Scholte-Stoneley wave.

## V. THE STIMULATION OF TRANSIENT LEAKY RAYLEIGH WAVES

In Fig. 5, there is also an anomaly at 7.95 MHz. It is known from almost similar calculations for harmonic waves in Ref. 18 that this anomaly corresponds to the generation of a Rayleigh wave. However, just as in the case of Fig. 4 there is no strong stimulation because the leaky feature is not

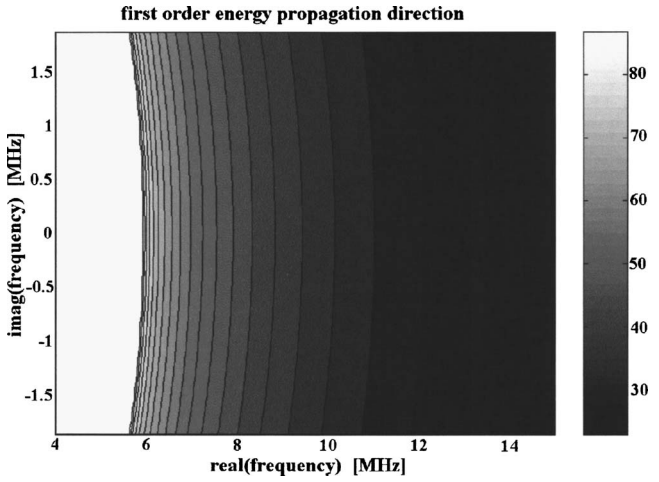


FIG. 10. Energy propagation direction of the first-order reflected waves.

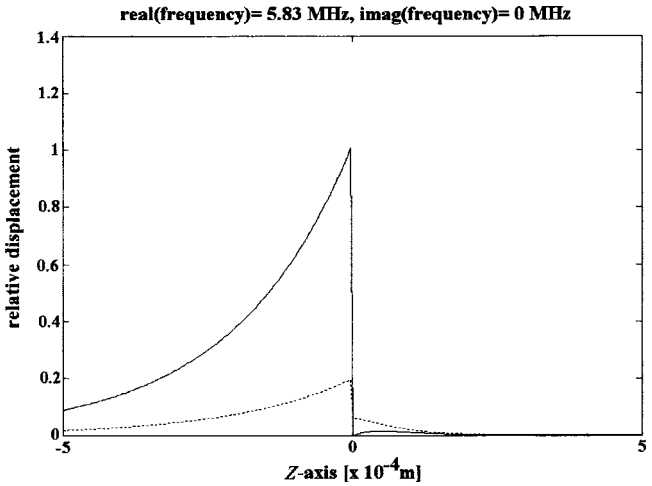


FIG. 11. Relative displacement amplitude for first-order transmitted and reflected sounds resulting from harmonic homogeneous plane waves incident on the considered periodically rough water-brass interface at normal incidence having a real frequency of 5.83 MHz. Solid line: $|\mathbf{u}_x|$; dotted line: $|\mathbf{u}_z|$. A typical Scholte–Stoneley wave profile is visible.

present. This leaky feature can only be there if incident harmonic inhomogeneous waves were used instead of "harmonic homogeneous plane waves."[18] Furthermore, the amplitudes in Fig. 13, which describe the wave field patterns for the first-order generated waves, are much smaller than the ones in Fig. 4. This shows why it is absolutely not beneficial to use a diffraction grating instead of a plane surface for the stimulation of Rayleigh waves by means of harmonic homogeneous plane waves. The next option is of course the use of inhomogeneous waves, as in Refs. 15–19 and 50. However, this has, up until now, only been practical in laboratory conditions and the generation of such waves is not really flexible.[16,19,20] The generation of "complex harmonic waves" is much more flexible. Therefore the question immediately arises if it is possible to use incident complex harmonic

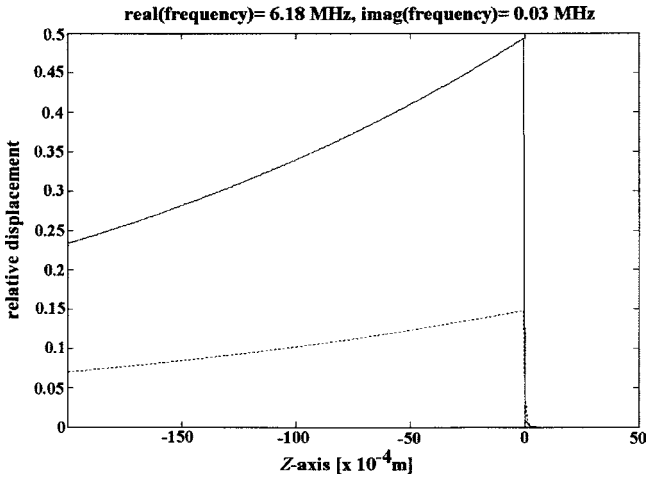


FIG. 12. Relative displacement amplitude for first-order transmitted and reflected sounds resulting from complex harmonic homogeneous plane waves incident on the considered periodically rough water-brass interface at normal incidence having a real frequency of 6.18 MHz and an imaginary frequency of 0.03 MHz. Solid line: $|\mathbf{u}_x|$; dotted line: $|\mathbf{u}_z|$. A typical Scholte–Stoneley wave profile is visible though it reaches much deeper into the liquid than in the harmonic case.

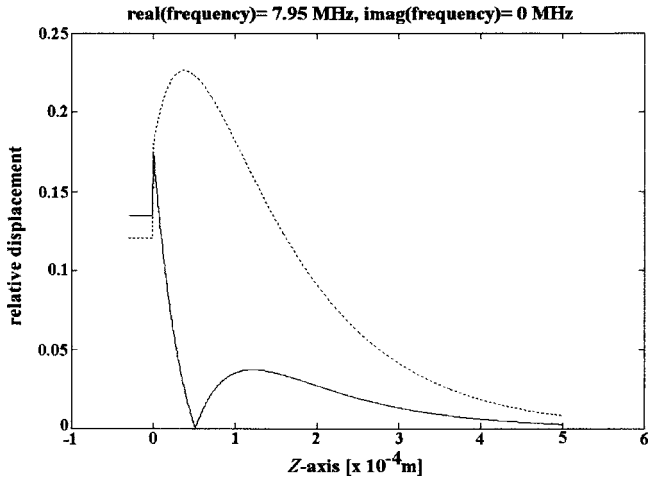


FIG. 13. Relative displacement amplitude for first-order transmitted and reflected sounds resulting from harmonic homogeneous plane waves incident on the considered periodically rough water-brass interface at normal incidence having a real frequency of 7.95 MHz. Solid line: $|\mathbf{u}_x|$; dotted line: $|\mathbf{u}_z|$. A typical Rayleigh wave profile is noticeable in the solid.

plane waves. For that purpose we have focused on the frequency area of 7.95 MHz. The results are seen in Figs. 14 and 15. For the possible stimulation of Rayleigh waves, it is necessary to look at Fig. 15, i.e., the first-order reflection coefficient. It is seen that four regions of importance are present, i.e., two amplitude peaks and two amplitude dips. Calculations have revealed that only the peak and the dip for negative imaginary frequency show Rayleigh features. Furthermore we found that the amplitude of the Rayleigh wave which corresponds to the peak for negative imaginary frequency has an amplitude that is more than 50 times the amplitude of the wave described in Fig. 4 at a plane interface. This shows that complex harmonic homogeneous plane waves are able to really stimulate Rayleigh waves on periodically corrugated surfaces and that it is therefore unnecessary to use more complicated harmonic inhomogeneous waves for that purpose. However, there is one important question that we would still like to answer, i.e., why does this stimulation occur? We have calculated the propagation direction in reflection for the Rayleigh wave corresponding to the

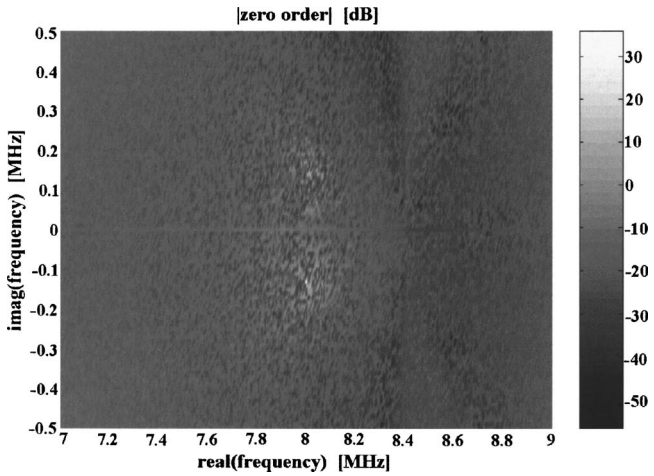


FIG. 14. A high-resolution closeup of Fig. 6 near the Rayleigh wave generating frequency.

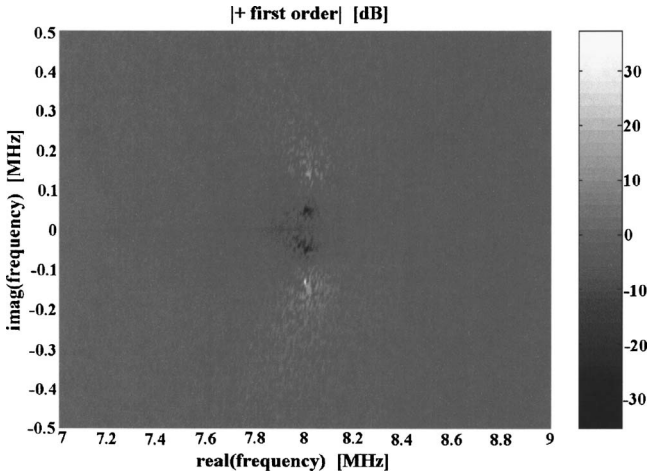


FIG. 15. A high-resolution closeup of Fig. 7 near the Rayleigh wave generating frequency.

peak for negative imaginary frequency. The result is 48° for both the phase propagation direction and the energy propagation direction. But this is not the only clue. Even though the amplitude distribution pattern for the sound field corresponding to the peak for negative imaginary frequency is the one of a leaky Rayleigh wave at a fixed position along the interface, it is completely different if one would also look at its variation along the interface. A leaky Rayleigh wave that is stimulated by means of a harmonic wave must have a decaying amplitude along the interface (because of energy leakage), whereas here the amplitude does not change at all along the interface. The reason is that, due to grating equation (20), no complex wave-vector components can be generated along the interface if the incident wave has none along the interface, which is the exact case here. However, due to the transient feature, here one must not just take a look in space but also in time. Because the amplitude for negative imaginary frequencies drops with increasing time, the amplitude would, if a part of the wave would be followed while it travels along the interface, have decreasing amplitude indeed. Consequently there is, if not just space but also time is considered, amplitude decay along the interface and that is the reason why the energy leaks at a calculated angle, equal to the Rayleigh angle. Therefore this is a transient leaky Rayleigh wave. For a positive imaginary frequency, however, there is no leakage but gain of energy while propagating, where the nature of this phenomenon is very different, and cannot be called a transient leaky Rayleigh wave. We have also performed calculations for oblique incidence, because for oblique incidence there is an imaginary part of the incident wave vector along the interface. We intended to figure out if this would be advantageous or not. The results which are not depicted here show that it is possible to generate leaky Rayleigh waves, but there is no strong stimulation and we have not found a relative displacement amplitude exceeding unity. Therefore we must conclude that for homogeneous plane waves, only normal incident complex harmonic waves are able to stimulate leaky Rayleigh waves.

## CONCLUSIONS

The diffraction of complex harmonic plane waves is described on a periodically corrugated interface between a liq-

uid and a viscoelastic isotropic solid. It is shown that contrary with harmonic homogeneous plane waves, complex harmonic homogeneous plane waves are not advantageous for stimulating Scholte-Stoneley waves, whereas they can be extremely advantageous for stimulating transient leaky Rayleigh waves. Furthermore, because the generation of complex harmonic plane waves is much more simple than the generation of harmonic inhomogeneous plane waves, the described technique is an important step forward in the practical generation of high-amplitude Rayleigh waves. This kind of wave is in its turn extremely important for NDT purposes of solids near the surface.

## ACKNOWLEDGMENT

One of the authors (N.F.D.) is a postdoctoral fellow of the research foundation—Flanders (FWO-Vlaanderen).

[1]J. M. Claeys, O. Leroy, A. Jungman, and L. Adler, J. Appl. Phys. **54**, 5657 (1983).
[2]J. M. Claeys and O. Leroy, Rev. Cethedec **72**, 183 (1982).
[3]A. Jungman, L. Adler, J. D. Achenbach, and R. Roberts, J. Acoust. Soc. Am. **74**, 1025 (1983).
[4]A. Jungman, O. Leroy, G. Quentin, and K. Mampaert, J. Appl. Phys. **63**, 4860 (1988).
[5]A. Jungman, L. Adler, and G. Quentin, J. Appl. Phys. **53**, 4673 (1982).
[6]K. Mampaert and O. Leroy, J. Acoust. Soc. Am. **83**, 1390 (1988).
[7]N. F. Declercq, R. Briers, J. Degrieck, and O. Leroy, IEEE Trans. Ultrason. Ferroelectr. Freq. Control **49**, 1516 (2002).
[8]N. F. Declercq, R. Briers, and O. Leroy, Ultrasonics **40**, 345 (2002).
[9]K. Mampaert, P. B. Nagy, O. Leroy, L. Adler, A. Jungman, and G. Quentin, J. Acoust. Soc. Am. **86**, 429 (1989).
[10]O. Leroy, B. Poirée, L. Sebbag, and G. Quentin, Acustica **66**, 84 (1988).
[11]L. Sebbag, thesis, University of Paris 7, 1987.
[12]O. Leroy, G. Quentin, and J. M. Claeys, J. Acoust. Soc. Am. **84**, 374 (1988).
[13]B. Poirée and L. Sebbag, J. Acoust. **4**, 21 (1991).
[14]G. Quentin, A. Derem, and B. Poirée, J. Acoust. **3**, 321 (1990).
[15]R. Briers and O. Leroy, J. Phys. IV **C1**, 679 (1992).
[16]W. Huang, R. Briers, S. I. Rokhlin, and O. Leroy, J. Acoust. Soc. Am. **96**, 363 (1994).
[17]R. Briers, Ph.D. thesis, Department of Sciences, KUL, 1995.
[18]K. E.-A. Van Den Abeele, R. Briers, and O. Leroy, J. Acoust. Soc. Am. **99**, 2883 (1996).
[19]R. Briers, O. Leroy, O. Poncelet, and M. Deschamps, J. Acoust. Soc. Am. **106**, 682 (1999).
[20]M. Deschamps and B. Hosten, Acustica **68**, 92 (1989).
[21]M. Deschamps, B. Poiree, and O. Poncelet, Wave Motion **25**, 51 (1997).
[22]M. Deschamps, B. Poiree, and O. Poncelet, Wave Motion **25**, 51 (1997).
[23]O. Poncelet and M. Deschamps, J. Acoust. Soc. Am. **102**, 292 (1997).
[24]A. Bernard, M. Deschamps, and M. J. S. Lowe, J. Acoust. Soc. Am. **107**, 793 (2000).
[25]N. F. Declercq, R. Briers, J. Degrieck, and O. Leroy, IEEE Trans. Ultrason. Ferroelectr. Freq. Control **52**, 776 (2005).
[26]N. F. Declercq, J. Degrieck, and O. Leroy, J. Appl. Phys. **97**, 054904 (2005).
[27]G. Wolken, J. Chem. Phys. **58**, 3047 (1973).
[28]M. Neviere, M. Cadilhac, and R. Petit, IEEE Trans. Antennas Propag. **AP21**, 37 (1973).
[29]J. L. Uretsky, Ann. Phys. (N.Y.) **33**, 400 (1965).
[30]N. Garcia and N. Cabrera, Phys. Rev. B **18**, 576 (1978).
[31]B. A. Lippmann, J. Opt. Soc. Am. **43**, 408 (1953).
[32]W. C. Meecham, J. Appl. Phys. **27**, 361 (1956).
[33]R. Petit, Nouv. Rev. Opt. **6**, 129 (1975).
[34]P. C. Waterman, J. Acoust. Soc. Am. **57**, 791 (1975).
[35]P. C. Waterman, J. Acoust. Soc. Am. **78**, 804 (1985).
[36]G. Whitman and F. Schwering, IEEE Trans. Antennas Propag. **25**, 869 (1977).
[37]A. Wirgin, Opt. Commun. **27**, 189 (1978).
[38]A. K. Jordan and R. H. Lang, Radio Sci. **14**, 1077 (1979).
[39]A. Wirgin, J. Acoust. Soc. Am. **68**, 692 (1980).
[40]N. F. Declercq, J. Degrieck, R. Briers, and O. Leroy, J. Appl. Phys. **96**, 6869 (2004).
[41]A. Teklu, M. A. Breazeale, N. F. Declercq, R. D. Hasse, and M. S. McPherson, J. Appl. Phys. **97**, 084904 (2005).
[42]N. F. Declercq, J. Degrieck, R. Briers, and O. Leroy, J. Acoust. Soc. Am. **116**, 3328 (2004); Ph. Ball, Nature News , 2004.
[43]N. F. Declercq, J. Degrieck, R. Briers, and O. Leroy, Ultrasonics **43**, 605 (2005).
[44]N. F. Declercq, J. Degrieck, and O. Leroy, Acta. Acust. Acust. **91**, 840 (2005).
[45]A. Atalar, J. Acoust. Soc. Am. **65**, 1101 (1979).
[46]J. M. Claeys and O. Leroy, J. Acoust. Soc. Am. **68**, 1894 (1980).
[47]A. Atalar, J. Acoust. Soc. Am. **70**, 1182 (1981).
[48]M. Deschamps, J. Acoust. Soc. Am. **96**, 2841 (1994).
[49]J.-M. Claeys, Ph. D. thesis, Department of Sciences, KUL, 1985.
[50]N. F. Declercq, J. Degrieck, R. Briers, and O. Leroy, Appl. Phys. Lett. **82**, 2533 (2003).
[51]M. Deschamps and C. L. Cheng, Ultrasonics **27**, 308 (1989).
[52]J. P. Charlier and F. Crowet, J. Acoust. Soc. Am. **79**, 895 (1986).
[53]M. Abramowitz and I. A. Stegun, *Hanbook of Mathematical Functions* (Dover, New York, 1972).